

Article

Comprehensive Assessment of Pollution Sources and Health Impacts in Suburban Area of Shanghai

Wan Wei ^{1,*}, Meng Wang ^{1,*}, Qi Yuan ¹, Zhuozhi Zhang ¹, Xinwei Li ¹, Shuwen Han ¹, Yusen Duan ², Qingyan Fu ² and Shun-Cheng Lee ^{1,*}

¹ Department of Civil and Environmental Engineering, The Hong Kong Polytechnic University, Kowloon, Hong Kong SAR, China; wanwei@polyu.edu.hk (W.W.); yq-qi.yuan@connect.polyu.hk (Q.Y.); zhuo-zhi.zhang@connect.polyu.hk (Z.Z.); xin-wei.li@connect.polyu.hk (X.L.); shuwen.han@connect.polyu.hk (S.H.)

² Shanghai Environmental Monitoring Center, Shanghai 200030, China; duanys@sheemc.cn (Y.D.); qingyanf@sheemc.cn (Q.F.)

* Correspondence: meng-cee.wang@polyu.edu.hk (M.W.); shun-cheng.lee@polyu.edu.hk (S.-C.L.)

Abstract: Shanghai, one of China's largest metropolises, faces significant environmental pollution challenges due to rapid economic development. Suburban areas of Shanghai are affected by both long-distance transport and local sources of pollutants. This study conducted an integrated analysis that links health-risk assessment of heavy metals and source apportionment of atmospheric constituents to distinguish the contributions of emission sources and the major sources of health risks. Source-apportionment analysis revealed that secondary sources had the greatest contribution to the local pollutants, indicating the significant influence of peripheral and long-distance transport. Health-risk assessment of Cr, Ni, As, and Cd revealed that local residents were exposed to respiratory health risks, in which Cr is the major contributor. This health risk was primarily associated with emissions from nearby industry-related sources. Our study highlights the significant effects of both long-distance transport and local source emissions on atmospheric composition and human health in large urban agglomerations. The findings can inform future efforts to develop more precise emission-reduction strategies and policy improvements to mitigate environmental pollution and protect public health.

Keywords: source apportionment; health-risk assessment; heavy metals; Shanghai; suburban area



Citation: Wei, W.; Wang, M.; Yuan, Q.; Zhang, Z.; Li, X.; Han, S.; Duan, Y.; Fu, Q.; Lee, S.-c.

Comprehensive Assessment of Pollution Sources and Health Impacts in Suburban Area of Shanghai. *Toxics* **2023**, *11*, 552. <https://doi.org/10.3390/toxics11070552>

Academic Editor: Yuan Cheng

Received: 15 May 2023

Revised: 15 June 2023

Accepted: 21 June 2023

Published: 23 June 2023



Copyright: © 2023 by the authors. Licensee MDPI, Basel, Switzerland. This article is an open access article distributed under the terms and conditions of the Creative Commons Attribution (CC BY) license (<https://creativecommons.org/licenses/by/4.0/>).

1. Introduction

Air pollution is typically considered as substances excessively emitted from both anthropogenic and natural sources, and which will pose a threat to atmospheric environment, regional climate, and human health when they accumulate in sufficient concentrations [1–3]. Due to rapid urbanization and industrialization, many developing countries, especially China, with its large population, are experiencing air-pollution incidents similar to those previously encountered in developed countries [4–6]. As a representative of China's metropolises, the cluster of cities along the route from Beijing to Shanghai is one of the most polluted areas in China, contributing 34% of the country's PM_{2.5} emissions with only 10% of its land area [7]. Shanghai, due to its geographical location in the Yangtze River Delta (YRD), is, inevitably, subject to regional pollution caused by the intensive industrialization [8–10].

A series of measures have been conducted by the government to improve the regional air quality in Shanghai, including the introduction of a series of laws and regulations, strict emission standards, and the adjustment of production structure, which have significantly improved the air quality in this region. However, regionalism and its complexity are still among the most pressing problems facing Shanghai and its surrounding areas [11–13]. Therefore, accurately identifying and quantifying the sources of ambient PM_{2.5} is crucial for implementing effective mitigation strategies, as well as reducing the impact on public

health and the environment. The positive matrix factorization (PMF) receptor model has been widely used in resolving different air-pollutant sources in the past decades [3,14–17]. However, PMF might introduce a significant amount of rotational ambiguity unique to the chosen factor resolutions [18,19]. In contrast, the multi-linear engine (ME-2) algorithm implemented within the Igor Pro software package is believed to be able to lead to a reduction in the rotational ambiguity and provide a rather unique solution [20,21]. It is also a powerful tool extensively employed for source apportionment [22–24].

Heavy metals, a group of elements commonly found in air pollutants, can be released into the atmosphere by various sources [25,26]. Although they might only comprise a small mass fraction of PM_{2.5}, they are considered to be one of the most important components causing aerosol toxicity [27]. Exposed to certain levels of heavy metals might result in a range of health problems, including respiratory diseases, internal organ damage, and it may affect the endocrine, immune, and nervous systems [26,28]. However, previous researches on health impacts of heavy metals mainly focused on individual cities, especially large cities. Suburban areas are often overlooked as they are considered to have relatively clean air. In actuality, suburban areas are often located downwind from urban areas and are vulnerable to the long-distance transport of pollutants from surrounding cities, especially in large city agglomerations such as the YRD region.

In this study, three winter months' worth of field observation and sampling was conducted at a suburban site of Shanghai from 2018 to 2019. Hourly time-resolved organic carbon (OC) and elemental carbon (EC) in PM_{2.5}, as well as 13 elements and 3 ions, were measured. The temporal variations and the source apportionment of these pollutions are discussed. Meanwhile, the health impacts of four main heavy metals (Cr, Ni, As, and Cd) were calculated and their possible sources were estimated. Our study provides valuable insights into the characteristics and trends of air pollution in suburban areas heavily affected by remote transmission from surrounding megacities or city agglomeration. These findings can inform the development of effective policies and strategies to reduce regional air pollution and protect human health.

2. Materials and Methods

2.1. Sampling Site

Field observation and sampling were conducted at Dianshan Lake (DSL) site, which is situated in the Qingpu District of western Shanghai and operated by the Shanghai Environmental Monitoring Center (Figure 1). This site is an ideal location for investigating the accumulation of local pollutants and long-distance transported pollution due to its geographical location, which intersects with Shanghai, Jiangsu, and Zhejiang provinces. Though it is near DSL and represents the environment of suburban Shanghai, it is considered to be affected by the industrial activities from surrounding areas, as well as the two highways beside it. Therefore, it is an ideal site to investigate the local pollutants accumulation and long-distance transported pollution [10].

2.2. Instruments and Measurements

In this study, ambient PM_{2.5} was detected over three winter months from November 2018 to February 2019. The mass concentrations of the samples were determined using a tapered-element oscillating microbalance monitor (TEOM, Thermo FH62C-14, Waltham, MA, USA) with a sampling flow rate of 16.7 L/min. The hourly measurement carried an uncertainty of ± 1.50 mg/m³, and the detection limit was 0.1 µg/m³. Consistent with a previous study [29], the concentration of PM_{2.5} was converted to hourly means. Water-soluble inorganic ions, such as sulfate and nitrate in PM_{2.5}, were measured by an online monitor for aerosols and gases (MARGA, model ADI2080, Metrohm Applikon B.V., Schiedam, The Netherlands).

Online measurements of OC and EC were conducted using a Sunset Semi-Continuous Carbon Analyzer (Sunset Laboratory, Forest Grove, OR, USA), which employs the thermal-optical transmittance method at a flow rate of 8 L/min. This method involves heating the sample to different temperatures in a controlled environment, and measuring the amount

of carbon released at each temperature. By comparing the amount of carbon released at different temperatures, it is possible to differentiate between organic and elemental carbon. Hourly time-resolved analyses of OC and EC were obtained using this instrument, with detection limits of 0.2 and 0.04 $\mu\text{g}/\text{m}^3$, respectively.



Figure 1. Location of sampling site (source: ©Apple Maps, <https://developer.apple.com/maps/web/> (accessed on 15 May 2023)).

2.3. Assessment of Health Risks of Heavy Metals

Health risk caused by heavy metals in PM is mainly carried in three ways: ingestion, inhalation, and dermal contact [26,27,30], of which inhalation is an important route of exposure, as the pulmonary bronchus is particularly vulnerable to exposure to $\text{PM}_{2.5}$ [31], and the heavy metals adsorbed therein are considered as a significant risk factor for lung cancer [32]. In this study, we used health-risk assessment models proposed by the United States Environmental Protection Agency (USEPA) to evaluate the health risk of four major toxic heavy-metal elements (Cr, Ni, As, and Cd) in $\text{PM}_{2.5}$ collected from the site. The average exposure amount via the inhalation pathway of each individual in a given time span can be calculated by Equation (1):

$$D_{inh} = (C \times IR \times EF \times DE) / (BW \times AT) \quad (1)$$

in which D_{inh} represents average daily dose for non-cancer risk or lifetime average daily dose for cancer risk ($\text{mg}/(\text{kg}\cdot\text{d})$); C represents heavy-metal element concentration in $\text{PM}_{2.5}$ (mg/m^3); IR represents respiration rate (m^3/d), take $17.6 \text{ m}^3/\text{day}$ as the average for the surveyed population across different age groups according to a previous study [30], and the subsequent parameters are also taken from this study; EF represents exposure frequency (d/year), take the average of 255 for different age groups; ED represents exposure duration (d), take the average of 70 for different age groups; BW represents body weight (kg), take 60 kg as the average value; and AT represents the averaging exposure time (d), $70 \times 365 \text{ d}$ was used for both carcinogens and non-carcinogens.

The hazard quotient (HQ) for non-carcinogenic risk and incremental lifetime cancer risk (ILCR) of inhalation exposure can be calculated, respectively [33]. The equations are:

$$\text{HQ} = D_{inh} / RfD \quad (2)$$

$$\text{ILCR} = D_{inh} \times SF \quad (3)$$

in which RfD is the reference dose which represents an estimate of daily exposure to the human population ($\text{mg}/(\text{kg}\cdot\text{day})$), 2.86×10^{-5} , 2.06×10^{-2} , 3.01×10^{-4} and 1.00×10^{-3} for Cr, Ni, As, and Cd, respectively [34]; SF is the cancer slope factor ($\text{mg}/(\text{kg}\cdot\text{d})$), take 42, 0.84, 15.1, and 6.3 for Cr, Ni, As, and Cd, respectively [34].

2.4. Source Apportionment Using the Tracer-Based Approach

The ME-2 algorithm was utilized to conduct the source apportionment in this study. The receptor model was performed using the source finder tool (SoFi v6.7) [21] within the Igor Pro software package (Wavemetrics Inc., Lake Oswego, OR, USA). Species input includes 2 carbonaceous materials, 3 water-soluble inorganic ions, 13 elements, and 8 health risk indices. In order to incorporate the health-risk factors (ILCR and HQ) into the source analysis and apportionment using ME-2, equivalent conversions of the original factors were performed based on the following equations:

$$ILCR_{conver} = 10 / -\log(ILCR_{ori}) \quad (4)$$

$$HQ_{conver} = 10 / -\log(HQ_{ori}) \quad (5)$$

After the equivalent conversions, the health-risk indices of the heavy metals input in the ME-2 algorithm are at the similar magnitude as the element concentrations (ng/m^3), avoiding the possible impact which may cause to the elemental analysis due to the direct addition of ILCR and HQ. Finally, the input matrix has a dimension of 2622×26 . The statistical data for the input species are summarized in Table S1. The elements of the measurement uncertainties (Unc) matrix were calculated by the following equation [35]:

$$Unc_{ij} = \sqrt{(DL_j)^2 + (CV_j x_{ij})^2} \quad (6)$$

where DL_j is the detection limit for compound j (DL_j was calculated as twice the standard deviation of the field blanks [36]); and CV_j is the coefficient of the variation for compound j .

In order to identify the ideal number of source factors, a series of rigorous tests were conducted, ranging from 1 to 10 factors. For each factor, 10 different random starting points were initialized to ensure the accuracy of the results. The Q/Q_{exp} ratio, usually used to measure the explanatory power of adding factors on the variation of the input dataset, decreased continuously from 12.9 to 1.91 when the number of factors increased from 1 to 10. The final number of factors was determined by the variation of Q/Q_{exp} ratio with the number of factors. As shown in Figure S1, the Q/Q_{exp} ratio displayed a smaller decrease when it is moving from 7 to 8 factors, suggesting 7 factors are sufficient to account for the variability present in the data [37,38]. Details of the evaluation can be found in our previous study [24]. The model can well match the variation of input species, as evidenced by high correlation values between modeled output and the input values. Specifically, the correlation analysis revealed a slope of 0.91 and R^2 of 0.96, which are presented in Figure S2.

3. Results and Discussion

3.1. Characteristics of Pollutants during the Sampling Period

As shown in Figure 2, the levels of pollutants fluctuated over the period, with clear peaks seen from 25 November–1 December in 2018, 14 January–4 February in 2019, and 23–26 February in 2019. Further investigation of the surrounding events and news revealed that these peaks corresponded to the middle and late periods of the China International Automobile Expo, the China Industry Expo and other large trade fairs, the traditional Chinese Spring Festival holiday and the late period of the Lantern Festival, respectively. Meanwhile, a serious haze occurred in Shanghai from 20 to 25 November in 2018. Such observation results indicate that the DSL area, as a junction of several large cities, is affected by the transport of surrounding pollutants while being affected by local emissions. The shaded areas in Figure 2 represent the weekends and legal holidays. It can be seen that during these non-working days high concentrations of pollutants accumulated at times, revealing that population flow and travel during non-working days do have an impact on suburban air quality, but other contributing factors are also involved.

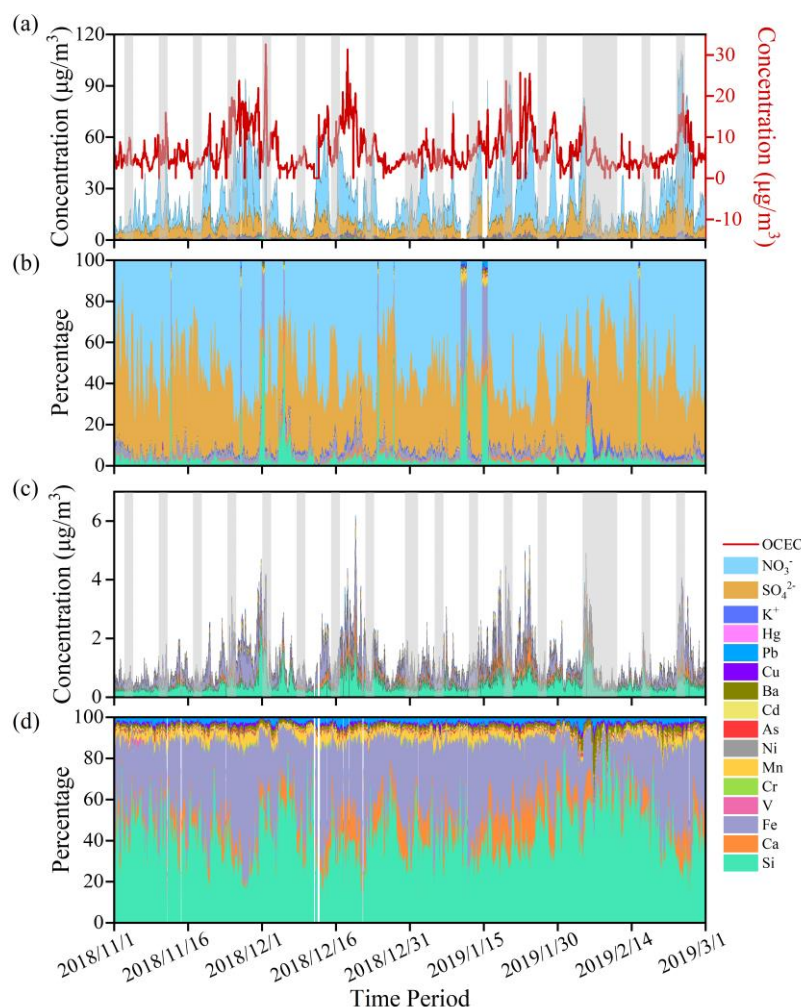


Figure 2. Temporal variations and distribution in all the detected pollutants (a,b), and the elements (c,d). The shaded areas represent the non-working days (weekends and legal holidays).

Temporal variations of all the pollutants observed are shown in Figure 2a. The total concentration of detected pollutants ranged from 11.62 to $208.42 \mu\text{g}/\text{m}^3$, with an average concentration of $49.55 \pm 36.60 \mu\text{g}/\text{m}^3$. However, this average concentration far exceeded the World Health Organization latest recommended air-quality guidelines ($5 \mu\text{g}/\text{m}^3$) [39], indicating significant potential environmental and health impacts for local residents.

The concentration distributions of all the pollutants are shown in Figure 2b. Overall, organic matter and water-soluble inorganic ions have the largest contribution to the $\text{PM}_{2.5}$ mass. Among them, NO_3^- represents the largest part of all the inorganic elements and ions detected, accounting for 62.93%. The concentration of NO_3^- ranged from 0.48 to $74.32 \mu\text{g}/\text{m}^3$ in these three winter months, with an average value of $15.21 \mu\text{g}/\text{m}^3$. The next is SO_4^{2-} , which varies from 0.86 to $33.35 \mu\text{g}/\text{m}^3$, with an average of $7.90 \mu\text{g}/\text{m}^3$, accounting for 32.69%. This is consistent with previous researches, which identified nitrates and sulfates as the primary inorganic components in Shanghai [40–42]. Simultaneously, it is also consistent with the overall trend that sulfate exhibited a decreasing trend over the past two decades, while nitrate displayed a clear increase [43]. If we focused on mainly the element, the result is displayed in Figure 2c,d. The contribution of these elements to local $\text{PM}_{2.5}$ is in the order: $\text{Fe} > \text{Si} > \text{Ca} > \text{Mn} > \text{Pb} > \text{Ba} > \text{Cu} > \text{As} > \text{Cr} > \text{Cd} > \text{Ni} > \text{Hg}$, which is not exactly consistent with the results observed at other suburban sites [27,28]. The most abundant elements are Fe, Si, and Ca, together accounting for 91.01% of all the elements, indicating the regional characteristic of air pollution in the suburban area of the YRD region.

3.2. Health-Risk Assessment

Four heavy metals (Cr, As, Ni, and Cd) were selected to evaluate HQ and ILCR to local residents. Based on previous studies, we have conducted a unified characterization of the health risks of different genders and age groups.

According to the non-carcinogenic hazard quotient, if $HQ < 1$, the non-carcinogenic risk to the human body is small or can be ignored. If $HQ > 1$, adverse health effects might exist in residential [44]. As shown in Table S2, the non-carcinogenic risks of four heavy metals were lower than the standard, and the total value was also within the acceptable range. However, among them, Cr is the major contributor, accounting for 87.1% of the total non-carcinogenic hazard (Table S2). Ni has the negligible non-carcinogenic risk compared to other elements, accounting for only 0.1%.

The total ILCR value of four main heavy-metal elements is 9.35×10^{-5} , which is higher than the safe risk threshold suggested by U.S. Environmental Protection Agency (10^{-6}) but within the recommended risk threshold (between 10^{-6} – 10^{-4}), demonstrating that the residents are, to a certain extent, exposed to the health risk through respiratory pathways. It is worth noting that, except Ni, concentrations of Cr, As, and Cd were all found to exceed the safe threshold for carcinogenic risks. Among the potentially carcinogenic elements under consideration, Cr posed the greatest cancer risk, accounting for 62.4% of the total cancer risks, and As was the second largest contributor (29.2%) (Table S2). As the temporal variations of the health-risk index shown in Figure S3, the ILCR value of Cr exceeded the maximum threshold in many periods, indicating great adverse health effects on the exposed residents.

3.3. Source Apportionment

As a suburban site, there is a combined effect of local pollution sources and surrounding pollutant transport. Seven potential sources of pollutants were identified using ME-2 and shown in Figure 3, including secondary sources, biomass burning, traffic-related sources, fugitive dust, industry-related sources, coal combustion, and heavy-oil combustion.

Factor 1 presents a high loading of NO_3^- and SO_4^{2-} , which are considered to be secondary nitrate and sulfate and associated with secondary sources [45,46]. Factor 2 shows high loading of K^+ and Ba. It is generally considered that K^+ is mainly from biomass burning [47–49]. The high percentage of Ba in this factor might indicate that the main crop burning near this area is wheat straw [50], which is consistent with the dominant crop type in the surrounding areas. Jiangsu and Anhui provinces, located nearby, are the major wheat-producing regions in the middle and lower reaches of the Yangtze River in China. After the harvest season, wheat straw is usually burned for disposal during late October to November. The high concentrations of Ba detected might have originated from these burning events which occurred during the observation period and their subsequent cumulative effects. Factor 3 is composed of high loadings of Cr, and moderate Mn, Ni, and Fe, which may point to the complex traffic-related sources. Among them, Cr is associated with the emission of lubricating oil, tailpipe emissions, and road abrasion [51]. Mn, Ni, and Fe could be partially from vehicular exhausts and the combustion of lubricating oil and fuel additives [52,53]. Higher EC loading than OC found in this factor also indicates the incomplete fuel combustion associated with vehicle emissions [54]. Factor 4 presents three characteristic peaks of Ca, Si, and Fe, with a moderate amount of Ba. These are generally considered to be crustal sources and derived from fugitive dust [55]. Factor 5 was characterized by high loadings of Cd and moderate Si and Hg. Cd usually originates from high-temperature processes in industry-related activities [56], such as industrial-process emissions or industrial coal combustion [57–59]. Different from the Si in Factor 4, 33.5% of Si here could be from large brick factories or concrete companies in the surrounding towns. Through the characterization of different types of stack gases from stationary sources, Zeng et al. indicated that high content of Si in air can also appear near glass factories, chemical factories, and cement factories [60]. Factor 6 is characterized by a high loading of As, moderate Pd, and high values of EC and OC. The elements are usually enriched

in coal [58]. Together with a high signal of organic-matter content, Factor 6 can reliably indicate coal combustion sources. Factor 7 is distinguished by a distinct high loading of V and a moderate Ni, which is considered a tracer for heavy-oil combustion, which includes the use of non-road machinery and shipping transportation [61,62].

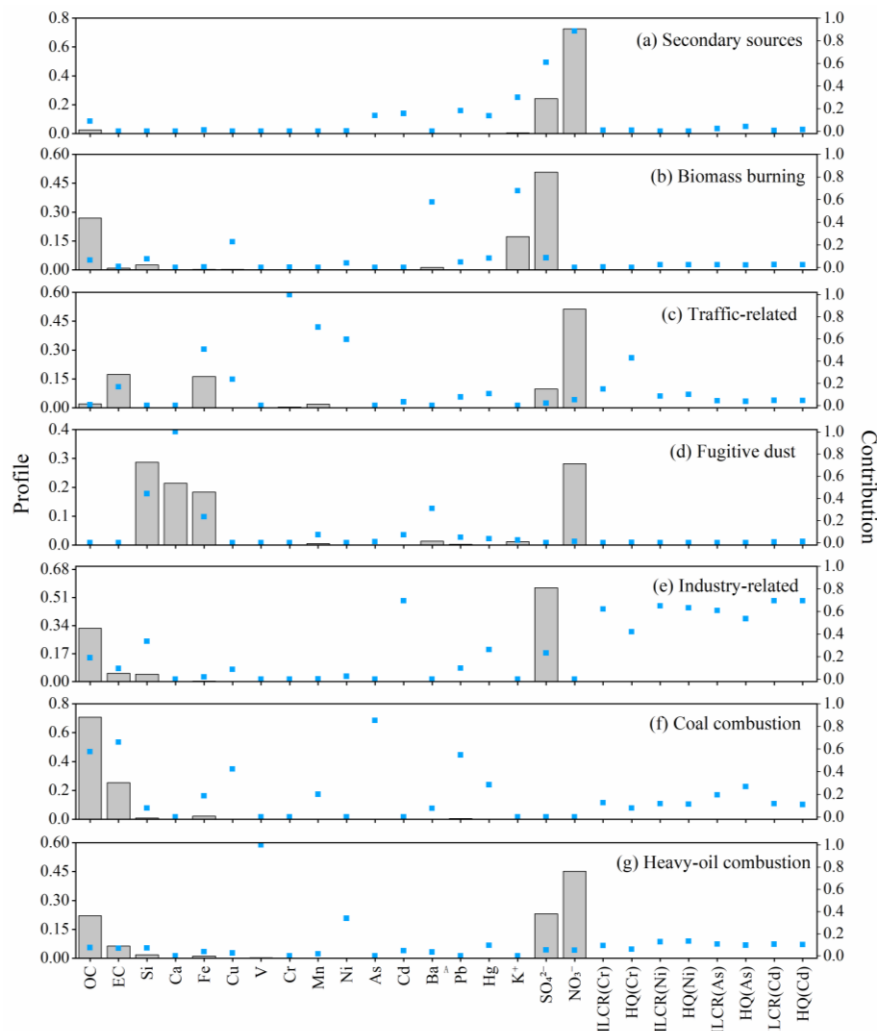


Figure 3. Seven factors identified by source apportionment. Factor profiles identified for all compounds and health-risk parameters (ILCR and HQ) for Cr, Ni, As, and Cd are displayed in the bar chart. The relative contribution of individual species to each factor is depicted by the blue dots.

The temporal and average contributions of seven identified sources are displayed in Figure 4. It can be observed that the secondary sources are the major contributors to the local atmospheric composition in every weekly statistics bar, and accounting for 60.5% of the total pollution sources. This indicated a significant influence of long-distance transport of pollutants from surrounding towns and urban areas. Important contributions from coal combustion and industry-related sources were also found, accounting for 13.4% and 9.7%, respectively. Fugitive dust was identified as the least significant contributor (2.0%). The percentage of different sources in the sampling period can be found in Figure S4.

The use of the lifetime-risk index in Figure 4 provides an intuitive visualization of the health hazards associated with heavy-metals exposure. The index is calculated as the sum of the equivalent converted HQ and ILCR values of four heavy metals. It can be observed that the lifetime-risk index generally displays a similar trend to the concentration of pollutants, although some discrepancies existed. This might suggest that certain heavy-metal elements and sources may be primarily responsible for the adverse effects on human health.

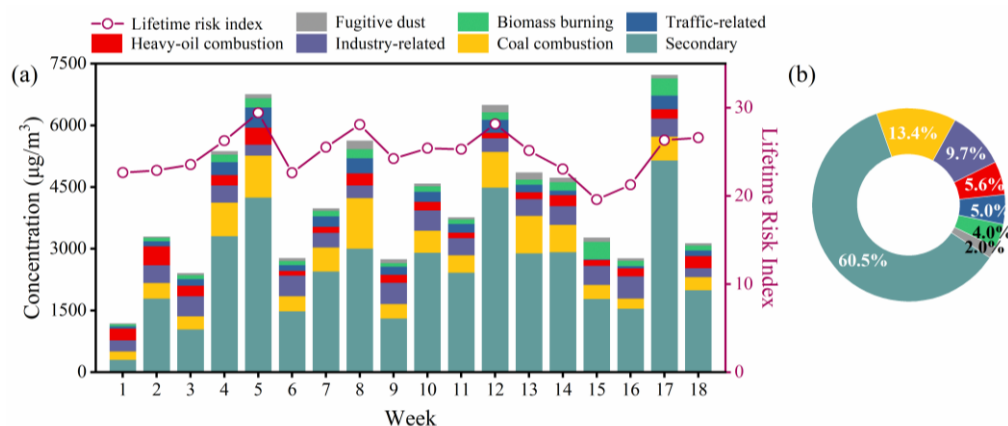


Figure 4. (a) Temporal variations of different sources. (b) The average contribution from the seven sources. The red line in (a) indicates the lifetime health-risk index, which is calculated by inhaled non-cancer hazard index (HQ) and increased lifetime cancer risk (ILCR).

3.4. Contribution of Different Sources to Health Risks

While using the ME-2 model for source apportionment, ILCR and HQ were simultaneously employed to allocate the health effects to different sources and quantify their respective contributions. It can be seen in Figure 5 that among all the sources, the total ILCR and HQ of four heavy metals emitted by industry-related sources are significantly higher than those from other sources. The three major contributors to carcinogenic risks were industry-related sources (64.3%), coal combustion (13.8%), and heavy-oil combustion (10.8%). As for the non-carcinogenic risks, industry-related sources remained the major contributor of non-carcinogenic risk among all the potentially sources (57.0%), followed by traffic-related (15.3%) and coal combustion (14.2%). Heavy metals in fugitive dust have the least harm to human health compared with other sources. The detailed contribution of the seven sources can be found in Table S3.

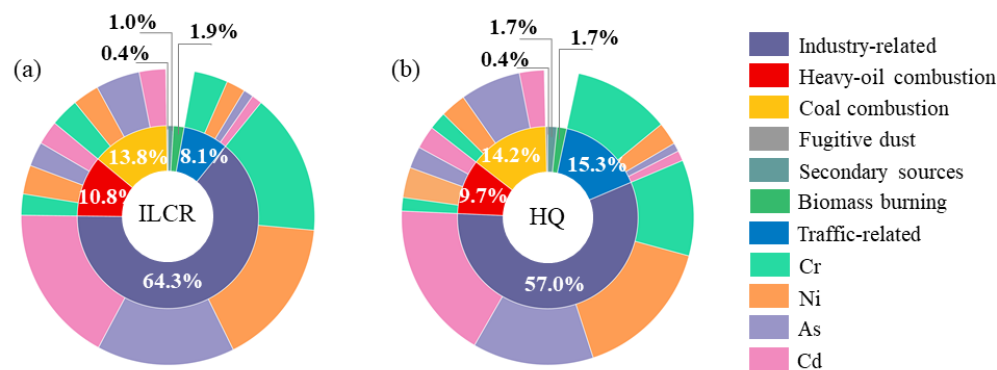


Figure 5. The contribution of different sources to health risks and contribution of four heavy-metal elements in each source.

It should be noted that, despite the relatively low contribution to the overall source apportionment (9.7%), industry-related sources have the potential to pose significant health risks to local residents. Specifically, the heavy metals emitted from surrounding industrial activities can contribute significantly to the metal-induced cancer risks faced by the local population. This is, to some extent, different from previous studies conducted in urban areas [27,63], which indicated traffic emission and coal combustion posed the predominant metal-induced health risk.

In fact, the contributions of different sources to both carcinogenic and non-carcinogenic risks associated with heavy metals exhibit regional characteristics, which can reflect the different industrial and energy structures [63]. In our study, the higher health risks associated

with industry-related emissions might be due to the gradual expansion of industrialization into suburban areas caused by the relocation of factories from urban to suburban regions. Additionally, as revealed in our study, the toxicity of secondary sources may not necessarily be higher than that of industry-related emissions, although it is the largest contribution to local pollutants. Therefore, future research on the primary toxic components and their sources is necessary to better understand the specific sources of health risks and develop more effective pollution-control strategies.

4. Conclusions

This study evaluated the pollution sources and associated health effects of PM_{2.5} detected during a three-month winter period in the suburban area of Shanghai. Secondary sources are the major contributor to local atmospheric components, accounting for more than 60% of the total pollutants, indicating the significant influence of long-distance transport from surrounding towns and urban areas. Health-risk assessment of Cr, Ni, As, and Cd revealed the local residents were exposed to respiratory carcinogenic risks induced by heavy metal. Cr posed the predominant impact, accounting for 62.4% for ILCR and 87.1% for HQ. By combining the health-risk assessment with source apportionment using the ME-2 model, we found that industrial-related emissions, which accounted for only 9.7% of the local aerosol components, were the predominant source of health risks for the residents, contributing to 64% of the metal-induced cancer risks. This could be attributed to the gradual expansion of industrialization into suburban areas caused by the relocation of factories. Our results emphasize the correlation between health-risk assessment of the primary toxic components and pollution concentration and source contribution may require further investigation for more accurate results. The findings of our study could provide scientific guidance to develop more precise pollution-control strategies and policy improvements that better protect public health.

5. Uncertainty of Health Risk Assessment

While efforts were expended to ensure the accuracy and reliability of the data, we acknowledge some limitations in this study. Firstly, exposure-risk assessment involves several parameters, including *IR*, *EF*, *ED*, and *BW*. However, this study calculates the average values for all age groups and genders to represent the overall health risk to human body, which may result in some discrepancies with previous studies. Additionally, gaps and omissions of data due to various objective factors and potential confounding factors that were not accounted for in the analysis may also affect the overall value calculations. Furthermore, we only focused on the risk assessment of four major heavy-metal elements. Therefore, the characterization of health risks in this study may be incomplete.

Future research should aim to expand the scope of the analysis to include a more comprehensive range of pollutants, in order to provide a more accurate and comprehensive assessment of the health risks associated with air pollution. The method of incorporating health-risk indexes into source apportionment also requires further refinement.

Supplementary Materials: The following supporting information can be downloaded at: <https://www.mdpi.com/article/10.3390/toxics11070552/s1>, Figure S1: The variation of Q/Q_{exp} with the increase number of factors; Figure S2: Scatterplot between the modeled output and the input values; Figure S3: Temporal variations of HQ and ILCR; Figure S4: Contribution of different sources; Table S1: Data statistics of the 26 species included in ME-2 analysis (ng/m³); Table S2: ILCR and HQ value of four heavy metals in PM_{2.5} in this study; Table S3: Contribution of seven identified sources to ILCR and HQ and the contributions of the four elements to each source.

Author Contributions: Conceptualization, W.W. and M.W.; data curation, W.W. and Q.Y.; investigation, Y.D.; methodology, M.W.; project administration, Q.F. and S.-C.L.; software, W.W.; supervision, Q.F. and S.-C.L.; visualization, W.W.; writing—original draft, W.W.; writing—review and editing, M.W., Z.Z., X.L., S.H. and S.-C.L. All authors have read and agreed to the published version of the manuscript.

Funding: This work was supported by the Start-up Fund for RAPs under the Strategic Hiring Scheme (P0043854), Green Tech Fund (GTF202110151), Environment and Conservation Fund-Environmental Research, Technology Demonstration and Conference Projects (ECF 63/2019), the RGC Theme-based Research Scheme (T24-504/17-N), the RGC Theme-based Research Scheme (T31-603/21-N), Key Research and Development Projects of Shanghai Science and Technology Commission (20dz1204000), and the State Ecology and Environment Scientific Observation and Research Station for the Yangtze River Delta at Dianshan Lake (SEED).

Data Availability Statement: The data from this study have been deposited in the Zenodo data archive with the DOI <https://doi.org/10.5281/zenodo.6473085> and are publicly available for research purposes [29].

Acknowledgments: We acknowledge the support of all the projects mentioned in this work. We also acknowledge the contribution of the State Ecology and Environment Scientific Observation and the Research Station for the Yangtze River Delta at Dianshan Lake.

Conflicts of Interest: The authors declare no conflict of interest.

References

1. Pan, Y.P.; Wang, Y.S. Atmospheric Wet and Dry Deposition of Trace Elements at 10 Sites in Northern China. *Atmos. Chem. Phys.* **2015**, *15*, 951–972. [[CrossRef](#)]
2. Pöschl, U. Atmospheric Aerosols: Composition, Transformation, Climate and Health Effects. *Angew. Chem. Int. Ed. Engl.* **2005**, *44*, 7520–7540. [[CrossRef](#)] [[PubMed](#)]
3. Ren, H.; Hu, W.; Yue, S.; Wu, L.; Ren, L.; Pan, X.; Wang, Z.; Sun, Y.; Kawamura, K.; Fu, P. Tracer-Based Characterization of Fine Carbonaceous Aerosol in Beijing during a Strict Emission Control Period. *Sci. Total Environ.* **2022**, *841*, 156638. [[CrossRef](#)] [[PubMed](#)]
4. Li, B.; Gasser, T.; Ciais, P.; Piao, S.; Tao, S.; Balkanski, Y.; Hauglustaine, D.; Boisier, J.-P.; Chen, Z.; Huang, M.; et al. The Contribution of China's Emissions to Global Climate Forcing. *Nature* **2016**, *531*, 357–361. [[CrossRef](#)] [[PubMed](#)]
5. Zhang, F.; Wang, Y.; Peng, J.; Chen, L.; Sun, Y.; Duan, L.; Ge, X.; Li, Y.; Zhao, J.; Liu, C.; et al. An Unexpected Catalyst Dominates Formation and Radiative Forcing of Regional Haze. *Proc. Natl. Acad. Sci. USA* **2020**, *117*, 3960–3966. [[CrossRef](#)]
6. An, Z.; Huang, R.-J.; Zhang, R.; Tie, X.; Li, G.; Cao, J.; Zhou, W.; Shi, Z.; Han, Y.; Gu, Z.; et al. Severe Haze in Northern China: A Synergy of Anthropogenic Emissions and Atmospheric Processes. *Proc. Natl. Acad. Sci. USA* **2019**, *116*, 8657–8666. [[CrossRef](#)]
7. China Power Team. Is Air Quality in China a Social Problem? Available online: <https://chinapower.csis.org/air-quality/> (accessed on 22 June 2023).
8. Liu, X.; Zou, B.; Feng, H.; Liu, N.; Zhang, H. Anthropogenic Factors of PM_{2.5} Distributions in China's Major Urban Agglomerations: A Spatial-Temporal Analysis. *J. Clean. Prod.* **2020**, *264*, 121709. [[CrossRef](#)]
9. Jia, H.; Huo, J.; Fu, Q.; Duan, Y.; Lin, Y.; Hu, X.; Fan, L.; Cheng, J. Atmospheric Characteristics and Population Exposure Assessment of Black Carbon at a Regional Representative Site in the Yangtze River Delta Region, China Based on the Five-Year Monitoring. *Sci. Total Environ.* **2021**, *777*, 145990. [[CrossRef](#)]
10. Shen, J.; Zhao, Q.; Cheng, Z.; Huo, J.; Zhu, W.; Zhang, Y.; Duan, Y.; Wang, X.; Antony Chen, L.-W.; Fu, Q. Evolution of Source Contributions during Heavy Fine Particulate Matter (PM_{2.5}) Pollution Episodes in Eastern China through Online Measurements. *Atmos. Environ.* **2020**, *232*, 117569. [[CrossRef](#)]
11. Zhang, X.Y.; Wang, Y.Q.; Niu, T.; Zhang, X.C.; Gong, S.L.; Zhang, Y.M.; Sun, J.Y. Atmospheric Aerosol Compositions in China: Spatial/Temporal Variability, Chemical Signature, Regional Haze Distribution and Comparisons with Global Aerosols. *Atmos. Chem. Phys.* **2012**, *12*, 779–799. [[CrossRef](#)]
12. Huang, X.; Ding, A.; Wang, Z.; Ding, K.; Gao, J.; Chai, F.; Fu, C. Amplified Transboundary Transport of Haze by Aerosol–Boundary Layer Interaction in China. *Nat. Geosci.* **2020**, *13*, 428–434. [[CrossRef](#)]
13. Chan, C.K.; Yao, X. Air Pollution in Mega Cities in China. *Atmos. Environ.* **2008**, *42*, 1–42. [[CrossRef](#)]
14. Ding, X.; He, Q.-F.; Shen, R.-Q.; Yu, Q.-Q.; Wang, X.-M. Spatial Distributions of Secondary Organic Aerosols from Isoprene, Monoterpenes, B-caryophyllene, and Aromatics over China during Summer. *J. Geophys. Res. Atmos.* **2014**, *119*, 11,877–11,891. [[CrossRef](#)]
15. Yue, S.; Zhu, J.; Chen, S.; Xie, Q.; Li, W.; Li, L.; Ren, H.; Su, S.; Li, P.; Ma, H.; et al. Brown Carbon from Biomass Burning Imposes Strong Circum-Arctic Warming. *One Earth* **2022**, *5*, 293–304. [[CrossRef](#)]
16. Wang, Q.; Liu, S.; Li, N.; Dai, W.; Wu, Y.; Tian, J.; Zhou, Y.; Wang, M.; Ho, S.S.H.; Chen, Y.; et al. Impacts of Short-Term Mitigation Measures on PM_{2.5} and Radiative Effects: A Case Study at a Regional Background Site near Beijing, China. *Atmos. Chem. Phys.* **2019**, *19*, 1881–1899. [[CrossRef](#)]
17. Liu, H.; Wang, Q.; Liu, S.; Zhou, B.; Qu, Y.; Tian, J.; Zhang, T.; Han, Y.; Cao, J. The Impact of Atmospheric Motions on Source-Specific Black Carbon and the Induced Direct Radiative Effects over a River-Valley Region. *Atmos. Chem. Phys.* **2022**, *22*, 11739–11757. [[CrossRef](#)]
18. Emami, F.; Hopke, P.K. Effect of Adding Variables on Rotational Ambiguity in Positive Matrix Factorization Solutions. *Chemom. Intell. Lab. Syst.* **2017**, *162*, 198–202. [[CrossRef](#)]

19. Paatero, P.; Hopke, P.K.; Song, X.-H.; Ramadan, Z. Understanding and Controlling Rotations in Factor Analytic Models. *Chemom. Intell. Lab. Syst.* **2002**, *60*, 253–264. [[CrossRef](#)]
20. Paatero, P.; Hopke, P.K. Rotational Tools for Factor Analytic Models. *J. Chemom.* **2009**, *23*, 91–100. [[CrossRef](#)]
21. Canonaco, F.; Crippa, M.; Slowik, J.G.; Baltensperger, U.; Prévôt, A.S.H. SoFi, an IGOR-Based Interface for the Efficient Use of the Generalized Multilinear Engine (ME-2) for the Source Apportionment: ME-2 Application to Aerosol Mass Spectrometer Data. *Atmos. Meas. Tech.* **2013**, *6*, 3649–3661. [[CrossRef](#)]
22. Crippa, M.; Canonaco, F.; Lanz, V.A.; Aijala, M.; Allan, J.D.; Carbone, S.; Capes, G.; Ceburnis, D.; Dall'Osto, M.; Day, D.A.; et al. Organic Aerosol Components Derived from 25 AMS Data Sets across Europe Using a Consistent ME-2 Based Source Apportionment Approach. *Atmos. Chem. Phys.* **2014**, *14*, 6159–6176. [[CrossRef](#)]
23. Fröhlich, R.; Crenn, V.; Setyan, A.; Belis, C.A.; Canonaco, F.; Favez, O.; Riffault, V.; Slowik, J.G.; Aas, W.; Aijälä, M.; et al. ACTRIS ACSM Intercomparison—Part 2: Intercomparison of ME-2 Organic Source Apportionment Results from 15 Individual, Co-Located Aerosol Mass Spectrometers. *Atmos. Meas. Tech.* **2015**, *8*, 2555–2576. [[CrossRef](#)]
24. Wang, M.; Wang, Q.; Ho, S.S.H.; Li, H.; Zhang, R.; Ran, W.; Qu, L.; Lee, S.; Cao, J. Chemical Characteristics and Sources of Nitrogen-Containing Organic Compounds at a Regional Site in the North China Plain during the Transition Period of Autumn and Winter. *Sci. Total Environ.* **2022**, *812*, 151451. [[CrossRef](#)] [[PubMed](#)]
25. Nriagu, J.O. Global Inventory of Natural and Anthropogenic Emissions of Trace Metals to the Atmosphere. *Nature* **1979**, *279*, 409–411. [[CrossRef](#)] [[PubMed](#)]
26. Du, Y.; Gao, B.; Zhou, H.; Ju, X.; Hao, H.; Yin, S. Health Risk Assessment of Heavy Metals in Road Dusts in Urban Parks of Beijing, China. *Procedia Environ. Sci.* **2013**, *18*, 299–309. [[CrossRef](#)]
27. Bi, C.; Chen, Y.; Zhao, Z.; Li, Q.; Zhou, Q.; Ye, Z.; Ge, X. Characteristics, Sources and Health Risks of Toxic Species (PCDD/Fs, PAHs and Heavy Metals) in PM_{2.5} during Fall and Winter in an Industrial Area. *Chemosphere* **2020**, *238*, 124620. [[CrossRef](#)]
28. Lv, W.; Wang, Y.; Querol, X.; Zhuang, X.; Alastuey, A.; López, A.; Viana, M. Geochemical and Statistical Analysis of Trace Metals in Atmospheric Particulates in Wuhan, Central China. *Environ. Geol.* **2006**, *51*, 121–132. [[CrossRef](#)]
29. Wang, M.; Duan, Y.; Xu, W.; Wang, Q.; Zhang, Z.; Yuan, Q.; Li, X.; Han, S.; Tong, H.; Huo, J.; et al. Measurement Report: Characterisation and Sources of the Secondary Organic Carbon in a Chinese Megacity over 5 Years from 2016 to 2020. *Atmos. Chem. Phys.* **2022**, *22*, 12789–12802. [[CrossRef](#)]
30. Xu, H.; Ho, S.S.H.; Cao, J.; Guinot, B.; Kan, H.; Shen, Z.; Ho, K.F.; Liu, S.; Zhao, Z.; Li, J.; et al. A 10-Year Observation of PM_{2.5}-Bound Nickel in Xi'an, China: Effects of Source Control on Its Trend and Associated Health Risks. *Sci. Rep.* **2017**, *7*, 41132.
31. Guo, Z.-Q.; Dong, W.-Y.; Xu, J.; Hong, Z.-C.; Zhao, R.-W.; Deng, C.-R.; Zhuang, G.-S.; Zhang, R.-X. T-Helper Type 1-T-Helper Type 2 Shift and Nasal Remodeling after Fine Particulate Matter Exposure in a Rat Model of Allergic Rhinitis. *Am. J. Rhinol. Allergy* **2017**, *31*, 148–155. [[CrossRef](#)]
32. Duan, S.; Zhang, M.; Sun, Y.; Fang, Z.; Wang, H.; Li, S.; Peng, Y.; Li, J.; Li, J.; Tian, J.; et al. Mechanism of PM_{2.5}-Induced Human Bronchial Epithelial Cell Toxicity in Central China. *J. Hazard. Mater.* **2020**, *396*, 122747. [[CrossRef](#)]
33. Hu, X.; Zhang, Y.; Ding, Z.; Wang, T.; Lian, H.; Sun, Y.; Wu, J. Bioaccessibility and Health Risk of Arsenic and Heavy Metals (Cd, Co, Cr, Cu, Ni, Pb, Zn and Mn) in TSP and PM_{2.5} in Nanjing, China. *Atmos. Environ.* **2012**, *57*, 146–152. [[CrossRef](#)]
34. Zhang, W.; Lv, S.; Liu, D.; Liu, P.; Yonmochi, S.; Wang, X.; Wang, Q. Distribution Characteristics of Heavy Metals in the Street Dusts in Xuanwei and Their Health Risk Assessment. *Environ. Sci.* **2015**, *36*, 1810–1817. [[CrossRef](#)]
35. Gianini, M.F.D.; Fischer, A.; Gehrig, R.; Ulrich, A.; Wichser, A.; Piot, C.; Besombes, J.-L.; Hueglin, C. Comparative Source Apportionment of PM₁₀ in Switzerland for 2008/2009 and 1998/1999 by Positive Matrix Factorisation. *Atmos. Environ.* **2012**, *54*, 149–158. [[CrossRef](#)]
36. Watson, J.G.; Chow, J.C.; Chen, L.-W.A.; Frank, N.H. Methods to Assess Carbonaceous Aerosol Sampling Artifacts for IMPROVE and Other Long-Term Networks. *J. Air Waste Manag. Assoc.* **2009**, *59*, 898–911. [[CrossRef](#)]
37. Brown, S.G.; Eberly, S.; Paatero, P.; Norris, G.A. Methods for Estimating Uncertainty in PMF Solutions: Examples with Ambient Air and Water Quality Data and Guidance on Reporting PMF Results. *Sci. Total Environ.* **2015**, *518–519*, 626–635. [[CrossRef](#)]
38. Wang, Q.; He, X.; Huang, X.H.H.; Griffith, S.M.; Feng, Y.; Zhang, T.; Zhang, Q.; Wu, D.; Yu, J.Z. Impact of Secondary Organic Aerosol Tracers on Tracer-Based Source Apportionment of Organic Carbon and PM_{2.5}: A Case Study in the Pearl River Delta, China. *ACS Earth Space Chem.* **2017**, *1*, 562–571. [[CrossRef](#)]
39. World Health Organization. *WHO Global Air Quality Guidelines: Particulate Matter (PM_{2.5} and PM₁₀), Ozone, Nitrogen Dioxide, Sulfur Dioxide and Carbon Monoxide*; World Health Organization: Geneva, Switzerland, 2021; ISBN 978-92-4-003422-8.
40. Zhu, C.; Cao, J.; Zhou, J.; Liu, S.; Dai, W.; Zhang, T.; Zhao, Z.; Shen, Z.; Li, H.; Wang, P. A Case Study of Chemical Characteristics of Daytime and Nighttime Ambient Particles in Shanghai, China. *Atmosphere* **2015**, *6*, 1141–1153. [[CrossRef](#)]
41. Yang, F.; He, K.; Ye, B.; Chen, X.; Cha, L.; Cadle, S.H.; Chan, T.; Mulawa, P.A. One-Year Record of Organic and Elemental Carbon in Fine Particles in Downtown Beijing and Shanghai. *Atmos. Chem. Phys.* **2005**, *5*, 1449–1457. [[CrossRef](#)]
42. Ye, B.; Ji, X.; Yang, H.; Yao, X.; Chan, C.K.; Cadle, S.H.; Chan, T.; Mulawa, P.A. Concentration and Chemical Composition of PM_{2.5} in Shanghai for a 1-Year Period. *Atmos. Environ.* **2003**, *37*, 499–510. [[CrossRef](#)]
43. Zhang, Y.; Tian, J.; Wang, Q.; Qi, L.; Manousakas, M.I.; Han, Y.; Ran, W.; Sun, Y.; Liu, H.; Zhang, R.; et al. High-Time-Resolution Chemical Composition and Source Apportionment of PM_{2.5} in Northern Chinese Cities: Implications for Policy. *EGUsphere* **2023**, preprint. [[CrossRef](#)]

44. U.S. Environmental Protection Agency. *Risk Assessment Guidance for Superfund Volume I Human Health Evaluation Manual (Part A) Interim Final*; U.S. Environmental Protection Agency: Washington, DC, USA, 2010.
45. Dai, Q.; Liu, B.; Bi, X.; Wu, J.; Liang, D.; Zhang, Y.; Feng, Y.; Hopke, P.K. Dispersion Normalized PMF Provides Insights into the Significant Changes in Source Contributions to PM_{2.5} after the COVID-19 Outbreak. *Environ. Sci. Technol.* **2020**, *54*, 9917–9927. [[CrossRef](#)] [[PubMed](#)]
46. Zhang, R.; Jing, J.; Tao, J.; Hsu, S.-C.; Wang, G.; Cao, J.; Lee, C.S.L.; Zhu, L.; Chen, Z.; Zhao, Y.; et al. Chemical Characterization and Source Apportionment of PM_{2.5} in Beijing: Seasonal Perspective. *Atmos. Chem. Phys.* **2013**, *13*, 7053–7074. [[CrossRef](#)]
47. Kim, S.-W.; Heo, J.; Bae, M.-S.; Kim, J.Y. PM_{2.5} Source Apportionment in Seoul, Korea: A Comparison of PMF and SMP Receptor Modeling Results. *Int. J. Environ. Sci. Technol.* **2023**, *20*, 2417–2426. [[CrossRef](#)]
48. Zhao, S.; Tian, H.; Luo, L.; Liu, H.; Wu, B.; Liu, S.; Bai, X.; Liu, W.; Liu, X.; Wu, Y.; et al. Temporal Variation Characteristics and Source Apportionment of Metal Elements in PM_{2.5} in Urban Beijing during 2018–2019. *Environ. Pollut.* **2021**, *268*, 115856. [[CrossRef](#)]
49. Heo, J.-B.; Hopke, P.K.; Yi, S.-M. Source Apportionment of PM_{2.5} in Seoul, Korea. *Atmos. Chem. Phys.* **2009**, *9*, 4957–4971. [[CrossRef](#)]
50. Ni, H.; Tian, J.; Wang, X.; Wang, Q.; Han, Y.; Cao, J.; Long, X.; Chen, L.-W.A.; Chow, J.C.; Watson, J.G.; et al. PM_{2.5} Emissions and Source Profiles from Open Burning of Crop Residues. *Atmos. Environ.* **2017**, *169*, 229–237. [[CrossRef](#)]
51. Jiang, N.; Liu, X.; Wang, S.; Yu, X.; Yin, S.; Duan, S.; Wang, S.; Zhang, R.; Li, S. Pollution Characterization, Source Identification, and Health Risks of Atmospheric-Particle-Bound Heavy Metals in PM₁₀ and PM_{2.5} at Multiple Sites in an Emerging Megacity in the Central Region of China. *Aerosol Air Qual. Res.* **2019**, *19*, 247–271. [[CrossRef](#)]
52. Ålander, T.; Antikainen, E.; Raunemaa, T.; Elonen, E.; Rautiola, A.; Torkkell, K. Particle Emissions from a Small Two-Stroke Engine: Effects of Fuel, Lubricating Oil, and Exhaust Aftertreatment on Particle Characteristics. *Aerosol Sci. Technol.* **2005**, *39*, 151–161. [[CrossRef](#)]
53. Thorpe, A.; Harrison, R.M. Sources and Properties of Non-Exhaust Particulate Matter from Road Traffic: A Review. *Sci. Total Environ.* **2008**, *400*, 270–282. [[CrossRef](#)]
54. Cao, J.-J.; Zhu, C.-S.; Tie, X.-X.; Geng, F.-H.; Xu, H.-M.; Ho, S.S.H.; Wang, G.-H.; Han, Y.-M.; Ho, K.-F. Characteristics and Sources of Carbonaceous Aerosols from Shanghai, China. *Atmos. Chem. Phys.* **2013**, *13*, 803–817. [[CrossRef](#)]
55. Li, R.; Wang, Q.; He, X.; Zhu, S.; Zhang, K.; Duan, Y.; Fu, Q.; Qiao, L.; Wang, Y.; Huang, L.; et al. Source Apportionment of PM_{2.5} in Shanghai Based on Hourly Organic Molecular Markers and Other Source Tracers. *Atmos. Chem. Phys.* **2020**, *20*, 12047–12061. [[CrossRef](#)]
56. Salma, I.; Maenhaut, W.; Záray, G. Comparative Study of Elemental Mass Size Distributions in Urban Atmospheric Aerosol. *J. Aerosol Sci.* **2002**, *33*, 339–356. [[CrossRef](#)]
57. Soleimani, M.; Amini, N.; Sadeghian, B.; Wang, D.; Fang, L. Heavy Metals and Their Source Identification in Particulate Matter (PM_{2.5}) in Isfahan City, Iran. *J. Environ. Sci.* **2018**, *72*, 166–175. [[CrossRef](#)]
58. Liu, P.; Ren, H.; Xu, H.; Lei, Y.; Shen, Z. Assessment of Heavy Metal Characteristics and Health Risks Associated with PM_{2.5} in Xi'an, the Largest City in Northwestern China. *Air Qual. Atmos. Health* **2018**, *11*, 1037–1047. [[CrossRef](#)]
59. Wang, J.; Pan, Y.; Tian, S.; Chen, X.; Wang, L.; Wang, Y. Size Distributions and Health Risks of Particulate Trace Elements in Rural Areas in Northeastern China. *Atmos. Res.* **2016**, *168*, 191–204. [[CrossRef](#)]
60. Zeng, X.; Kong, S.; Zhang, Q.; Ren, H.; Liu, J.; Feng, Y.; Yan, Q.; Qin, S.; Zheng, S.; Yao, L.; et al. Source Profiles and Emission Factors of Organic and Inorganic Species in Fine Particles Emitted from the Ultra-Low Emission Power Plant and Typical Industries. *Sci. Total Environ.* **2021**, *789*, 147966. [[CrossRef](#)]
61. Zhao, M.; Zhang, Y.; Ma, W.; Fu, Q.; Yang, X.; Li, C.; Zhou, B.; Yu, Q.; Chen, L. Characteristics and Ship Traffic Source Identification of Air Pollutants in China's Largest Port. *Atmos. Environ.* **2013**, *64*, 277–286. [[CrossRef](#)]
62. Tao, J.; Zhang, L.; Cao, J.; Zhong, L.; Chen, D.; Yang, Y.; Chen, D.; Chen, L.; Zhang, Z.; Wu, Y.; et al. Source Apportionment of PM_{2.5} at Urban and Suburban Areas of the Pearl River Delta Region, South China—With Emphasis on Ship Emissions. *Sci. Total Environ.* **2017**, *574*, 1559–1570. [[CrossRef](#)]
63. Xie, J.; Jin, L.; Cui, J.; Luo, X.; Li, J.; Zhang, G.; Li, X. Health Risk-Oriented Source Apportionment of PM_{2.5}-Associated Trace Metals. *Environ. Pollut.* **2020**, *262*, 114655. [[CrossRef](#)]

Disclaimer/Publisher's Note: The statements, opinions and data contained in all publications are solely those of the individual author(s) and contributor(s) and not of MDPI and/or the editor(s). MDPI and/or the editor(s) disclaim responsibility for any injury to people or property resulting from any ideas, methods, instructions or products referred to in the content.